Development of a mobile fast-screening laser-induced breakdown detection (LIBD) system for field-based measurements of nanometre sized particles in aqueous solutions

Christopher Latkoczy,[a] Ralf Kägi,*[a] Martin Fierz,[b] Mathias Ritzmann,[a] Detlef Günther[c] and Markus Boller[a]

Received 29th January 2010, Accepted 1st April 2010
First published as an Advance Article on the web 28th April 2010
DOI: 10.1039/c002020f

Laser-induced breakdown detection (LIBD) is a promising method to detect trace amounts of nanoparticles (NP, <100 nm) in aqueous suspensions. Based on available systems, we developed a mobile LIBD, designed for on-site and on-line measurements. We used the energy ratio of every laser pulse before and after passing the laser beam through the aqueous sample as a new method to detect laser-induced plasma events. The particle size and the particle number density are derived from recorded energy curves. Our LIBD is operated with a Nd:YAG laser at 100 Hz significantly reducing the measurement times compared to other LIBD systems operated at 20 Hz and increasing the capabilities for monitoring purposes. Long-term experiments on water samples revealed losses of NP up to 75% in 15 mL and 35% in 5 L sample containers after 3 months. The size of the particles remained constant (5 L) or slightly decreased (15 mL) indicating significant adsorption of NP to the walls of the sampling containers. Furthermore, we monitored the NP content of water after different purification steps at a drinking water plant (Maennedorf, Lake Zurich, Switzerland). Activated carbon filtration resulted in an increase of the particle size from ~20 nm to ~75 nm possibly caused by the release of organic fragments derived from the biology within the activated carbon tank. After the final ultrafiltration step the particle size was around 10 nm in agreement with the nominal cutoff of 100 kDa of the membrane. The results underline the strength of a fast-screening LIBD to detect relative changes in NP size and concentration.

1. Introduction

With the current advances of nanotechnology, the environment will be increasingly exposed to engineered nanosized materials (including engineered nanoparticles (ENPs)) released either intentionally (*e.g.* remediation strategies) or accidentally (*e.g.* surface abrasion and elutriation from textiles as well as leakage from or damages in production facilities). When ENP enter the aquatic environment, the rapid dilution and aggregation with other colloids make it extremely challenging to trace such materials. Thus, nanoparticle emissions should preferably be controlled and monitored directly at the emission source in a similar way as it is already performed for monitoring of airborne NP.[1,2]

Besides this emerging topic of ENP released to the environment, there are a high number of (natural) colloids (defined here as submicron particles) already present in the aquatic media. Although natural colloids have been known for a long time and their importance has been recognized, sizing and 'counting' colloids with a diameter at the lower size range (<100 nm) in surface waters are still very difficult or even impossible using commercially available techniques.[3–5] Dedicated single particle counters cannot detect particles <40 nm (PMS, Colorado, USA), and are designed to detect trace impurities in ultraclean water

[a]*Eawag, Swiss Federal Institute for Aquatic Science and Technology, Ueberlandstrasse 133, CH-8600 Duebendorf, Switzerland. E-mail: ralf.kaegi@eawag.ch*
[b]*University of Applied Sciences Northwestern Switzerland, School of Engineering, Institute of Aerosol and Sensor Technology, Klosterzelgstrasse 2, CH-5210 Windisch, Switzerland*
[c]*ETH Zurich, D-CHAB, Laboratory of Inorganic Chemistry, Wolfgang-Pauli-Strasse 10, CH-8093 Zurich, Switzerland*

Environmental impact

Increased production volumes of nanoparticles (NPs) and their application in a wide range of products will inevitably lead to a proliferation of NP in the aquatic environment, with currently unknown consequences. This calls for the development of analytical devices capable of on-line monitoring NP in aqueous matrices.
Based on existing systems, we have refined the laser induced breakdown detection (LIBD) technique, focusing on fast on-line measurements. We monitored the NP content in the drinking water at different purification steps in water works. The results demonstrate the strength of our LIBD system to detect and quantify small changes in NP size and concentration in aqueous suspension.

used for example in the semiconductor industry, thus requiring immense dilution ratios when applied to natural systems. The recently introduced NTA (nanoparticle tracking analysis, NanoSight Ltd, UK) technique tracks individual particles based on their scattered light and calculates the hydrodynamic diameters of individual particles based on the derived diffusion coefficients. The NTA yields complete size distributions and can detect particles down to 10 nm (depending on the material). However, as on-line measurements would be very challenging this technique can hardly be used for monitoring purposes.

Thus, there is a need for measurement devices that can detect particles down to the nanometre size range and additionally can be operated on-site and on-line for monitoring purposes. The laser induced breakdown detection (LIBD) is a very promising technique capable of detecting trace amounts of NP down to about 10 nm, invented by Japanese researchers.[6,7] Further improvements of the methods included the refinement of the plasma detection (acoustical[8] or optical detection[9,10]) as well as deriving particle size distributions from recorded LIBD data.[11,12] Recently Kim and Walther[13] and Walther and Hauser[14] reviewed the LIBD technique. The measurement principle is based on a pulsed laser beam that is focused on a measurement cuvette containing the NP in suspension. When the laser pulse power density exceeds a certain breakdown threshold (=ionization potential), a breakdown of the dielectric properties occurs and subsequently a plasma forms. The breakdown and thus the formation of the plasma occur selectively on the particles as the laser power density (E^0) needed to ignite a plasma in solids is lower than for liquids (solvent) and for gases (gas bubbles) ($E^0_{solid} < E^0_{liquid} < E^0_{gas}$). Furthermore, the laser power density needed to induce a breakdown shows a size dependence; smaller particles need a higher power density than larger particles of the same material ($E^0_{small} > E^0_{large}$).[15] The rapid expansion of the plasma (i) creates an acoustic signal, (ii) radiates light in the visible wavelength and (iii) absorbs and scatters the incoming laser light (inverse Bremsstrahlung, photoionization and Thomson scattering). All these effects can be used to detect the plasma. The first effect is referred to as optical detection method,[16–18] the second as acoustic detection method[6,7,19] and the third effect is for the first time explored in this paper. The breakdown probability (BDP) is defined as the fraction of laser shots that resulted in plasma formation (*i.e.* number of plasma events detected/total number of laser pulses). Recording the BDP as a function of the laser energy that is increased stepwise results in so-called energy curves. The size, number and also the size distribution of NP contained in suspension can be derived by analyzing the energy curves or selected parts thereof.[13]

In this study we present an LIBD system based on a new plasma detection method (energy ratios between incoming and outgoing laser pulses), later referred to as energy ratio LIBD that is operated at a repetition rate of 100 Hz. In order to validate the results of the energy ratio LIBD, we have additionally implemented the well-established optical detection method in our LIBD system. To show the capabilities of the LIBD to detect relative changes in NP content and to underline the advantage of on-site and on-line analyses two sets of experiments were performed. In the first set the time dependent loss of NP contained in raw lake water to different sample containers was quantified and in a second set of experiments, we monitored the NP content of water after different treatment steps in water works.

2. Experimental methods

2.1. Standard reference materials

For the size and concentration calibrations we used NIST traceable size standards covering the size range between 20 and 500 nm (Duke Scientific Corporation, USA, 3000 Series Nanospheres). The standards were stored in the dark at room temperature. The dilution of the standards to the desired concentrations was performed in a clean room environment.

To dilute the stock solutions 18.2 MΩ cm resistivity ultrapure water (Milli-Q, Element system, Millipore, Switzerland) was used. The same water quality was also used to perform blank measurements.

All bottles for water collection at the water works were acid washed using nitric acid and hydrochloric acid. The bottles were rinsed using ultrapure water and filled with 1 wt% nitric acid for storage. All bottles were rinsed with the water of interest before collecting the water sample. Water samples were transported back to the laboratory in a cool box.

2.2. Laser induced breakdown detection (LIBD) system

The schematic diagram and our LIBD instrumentation designed for on-site measurements are given in Fig. 1. Fig. 2 shows a photograph of the system. In the current setup, we use a pulsed Nd:YAG laser (Quantel CFR 200, TEM00 mode, laser wavelength = 532 nm, max pulse energy = 6 mJ, max repetition rate: 100 Hz, beam diameter: 1.5 mm, pulse duration: 13 ns, beam divergence < 1.5 mrad). The energy of each individual laser pulse is recorded using two different pyroelectric detectors (PE09-SH and PE10-SH, Ophir Optronics, Jerusalem, Israel) located in front of and behind the sample cell. The laser beam is directed with a 1 : 10 beam splitter to the first pyroelectric detector (PE09-SH) to monitor the incoming laser energy. The second pyroelectric detector (PE10-SH), which is placed in axis behind the sample cell, records the transmitted laser energy. The laser pulse energy is adjusted by a movable $\lambda/2$ zero-order waveplate and a fixed Glan-Laser calcite polarizer based on the incoming laser energy recorded at the first energy detector.

Energy curves are always related to the energy recorded at the first energy detector as the laser power density can directly be related to the energy recorded at the first energy detector at fixed focusing conditions and laser parameters. Since the synchronization of the two pyroelectric detectors is crucial, the trigger

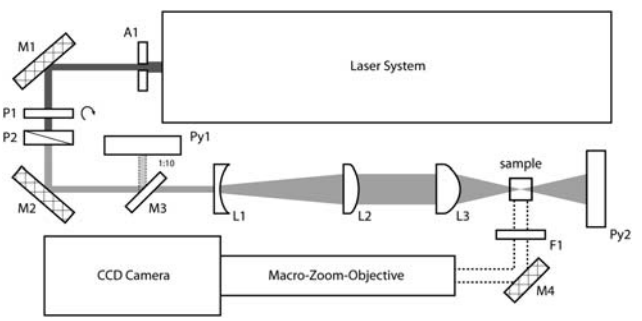

Fig. 1 Design of the mobile laser-induced breakdown detection system with optimized beam path and compact laser system.

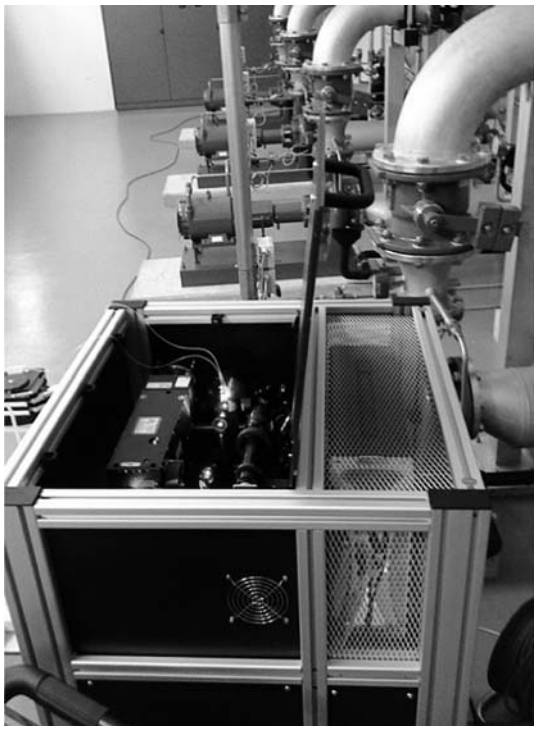

Fig. 2 LIBD instrumentation for field-based measurements.

signal from the Q-switch of the laser was used as the master trigger signal to control each individual pyroelectric detector. The timing of the complete system is programmed on-board using a reconfigurable I/O (RIO) FPGA technology provided by National Instruments. The laser beam is focused into the rectangular quartz sample cell (100-QS, volume = 3500 μL, Hellma Schweiz AG, Zumikon, Switzerland) utilizing a three-lens setup (plano-concave, plano convex lens and positive meniscus lens) to expand, collimate and focus the laser beam. The final lens setup was adjusted according to numerical calculations of the propagation and the resulting power density distribution of a Gaussian-shaped (TEM00-mode) laser beam through the three-lens setup using Optica 3 (Optica software, Illinois, USA) considering spherical aberrations of all lenses. The sample cell is tightly fitted into a sample holder to guarantee reproducible positioning of the sample cell, perpendicular to the laser beam. For on-line measurements, this sample cell is replaced by a flow cell (Hellma Schweiz AG, Zumikon, Switzerland) with a much smaller inner volume (300 μL), but the same geometrical dimensions (12.5 × 12.5 × 45 mm). The flow rate is adjusted using a peristaltic pump and is set to 2 mL min^{-1} for this study. An in-house control and evaluation software were designed and developed using a full featured National Instrument LabVIEW™ software environment. The system can be controlled remotely *via* a wireless connection, which enhances the capabilities for field-based measurements. Furthermore, the novel energy ratio LIBD allows a simplified instrumental setup, important for on-site measurements.

2.3. Optical detection method

The laser-induced plasma is spatially recorded using a monochrome full picture CCD video camera (648 × 488 pixels; Basler piA640-200gm) in combination with a macro-zoom-objective (Rodenstock, ROD 0.8-4), similar to the approach described by Bundschuh *et al.*[16] The location (center of mass) of individual plasma events was determined using on-line image-processing software (National Instrument LabVIEW™ Vision). Recording a large number of plasma events (typically 2000–5000) and plotting the center of mass of the individual plasma events as *x*–*y* scatter diagrams results in a cloud that includes all the plasma locations. The magnitude of that cloud in the beam direction (referred to as ignition length) is a measure of the particle size.[16] In this study, however, the optical setup is only used to detect the individual plasma events and the ignition length is not further explored.

2.4. Energy ratio detection method

The energy ratio of laser pulse recorded in front of and behind the sample cell can alternatively be used to detect individual plasma events. A constant energy ratio of about 8 is obtained in our system under the condition of no plasma formation. In case of a plasma event, the transmitted energy is reduced due to energy absorption (inverse Bremsstrahlung, photoionization) and interactions of the plasma with the laser beam (Thomson scattering) resulting in a decreased energy recorded at the pyroelectric detector behind the measurement cell. This leads to a decrease in the ratio between the recorded transmitted and incoming laser energies. The threshold ratio used to identify plasma events is based on the energy ratio measured when no plasma occurs and allowing an additional deviation of 4% due to energy fluctuations and the laser stability. To illustrate this approach, three experiments (1000 laser pulses each) using monodisperse reference polystyrene nanospheres ranging from 19–97 nm were carried out and the energy ratio histograms are shown in Fig. 3. The laser energy was adjusted to reach a BDP of

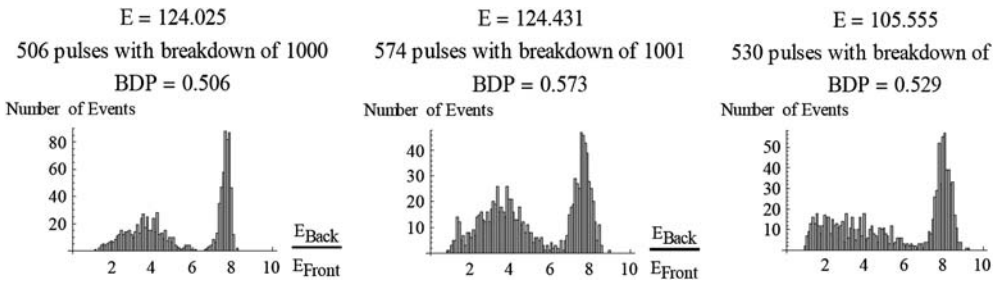

Fig. 3 Energy ratio histograms for three different particle sizes (19 nm, 46 nm, 97 nm) recorded with a breakdown probability of around 50% (the energy values in the graphs are reported in μJ, as recorded at the first energy detector).

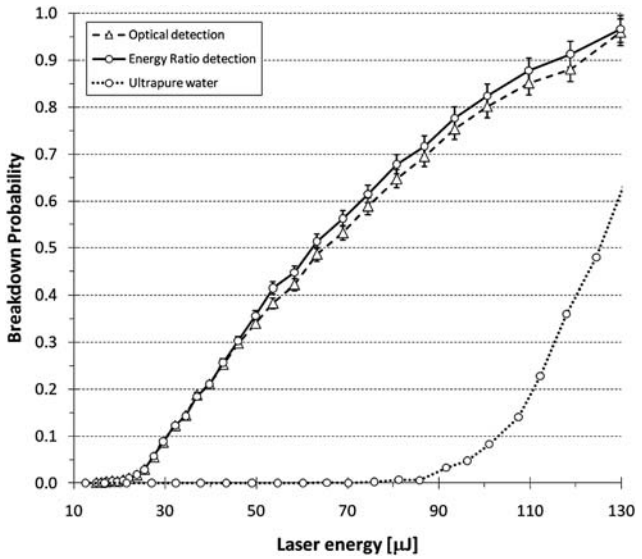

Fig. 4 Comparison of energy curves obtained with energy ratio LIBD and optical LIBD, respectively. A standard solution containing polystyrene reference materials with a particle size of 151 ± 4 nm and a concentration of 5.1×10^7 NPS mL^{-1} was measured three times individually within the respective detection mode.

around 0.5. A clear separation between energy ratios recorded in the presence and in the absence of plasma events can be observed.

In Fig. 4 the results obtained using the energy ratio LIBD are compared with the results from the optical LIBD. The obtained energy curves are identical in the lower part of the energy curve (<35% BDP). At higher energies the optical detection method yields slightly lower BDP, however, the differences are still within the measurement uncertainties.

3. Calibration of the LIBD system

3.1. Calibration of the particle size

The initial rise of the energy curves, referred to as threshold energy (E_{th}), is a measure of the particle size. Thus, a size calibration can be derived by recording energy curves of monodisperse particle standards of different sizes and estimating the respective threshold energy.[15] The recorded energy curves are given in Fig. 5. The lower part of the energy curves was best described with a logistic function. We, thus used this approach to fit the lowest part of the energy curves (up to BDP = 0.1) which allowed us to determine the energy at a BDP of 0.02, used to approximate E_{th}. The size calibration curve using standards from 21–499 nm is given in Fig. 6. The data can be fitted using an exponential fit function (eqn (1)):

$$d_{particle} = 1100e^{-0.094 \times E_{th}} \quad (1)$$

with $d_{particle}$ = particle diameter in nm and E_{th} = the laser energy in µJ for a BDP of 0.02. Our E_{th} values are about a factor of 2 lower compared to the values reported by Walther *et al.*[15] The different laser optical setups and the different laser focus properties most likely account for the observed differences together with the fact that we determined our E_{th} values at a BDP of 0.02 compared to 0.01.[15] Due to the better counting statistics we preferred using a BDP of 0.02 instead of 0.01 to derive the E_{th} values. It has to be kept in mind that the underlying assumption for the determination of the particle size using the energy threshold method is a monodisperse particle size distribution. Natural systems, however, are highly polydisperse and the results will be biased towards larger particle sizes.

3.2. Calibration of the particle concentration

For the determination of the particle number density (*i.e.* number of particles per unit volume), we used the algorithm based on a statistical model proposed by Scherbaum *et al.*[20] A key parameter in this model is the effective focal volume (V_{eff}) describing the volume within which a particle of a certain size will be excited by a laser pulse exceeding the respective power density or in other words it describes the spatial extent (=volume) of a certain laser power density. Scherbaum *et al.*[20] approximated this volume with a rotational ellipsoid, although this simplification has its limitations mainly due to lens imperfections

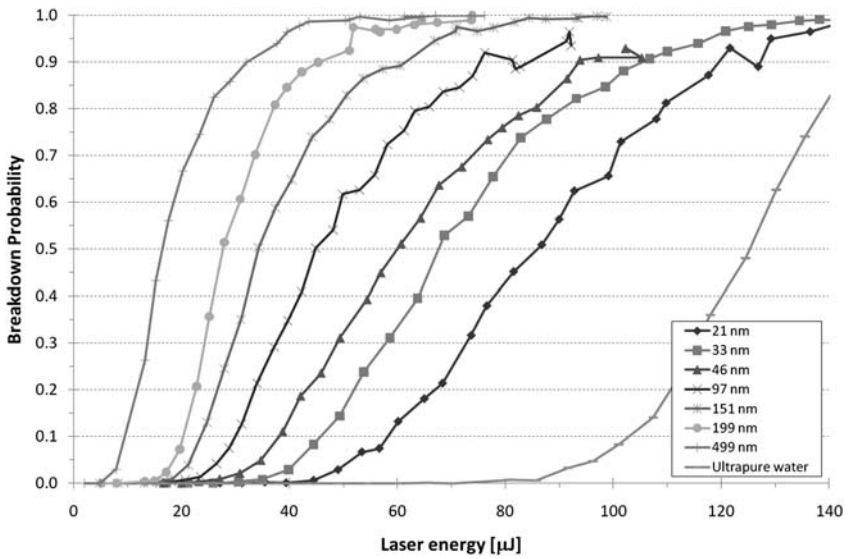

Fig. 5 Energy curves for a given set of polystyrene nanospheres with a diameter range from 21–499 nm.

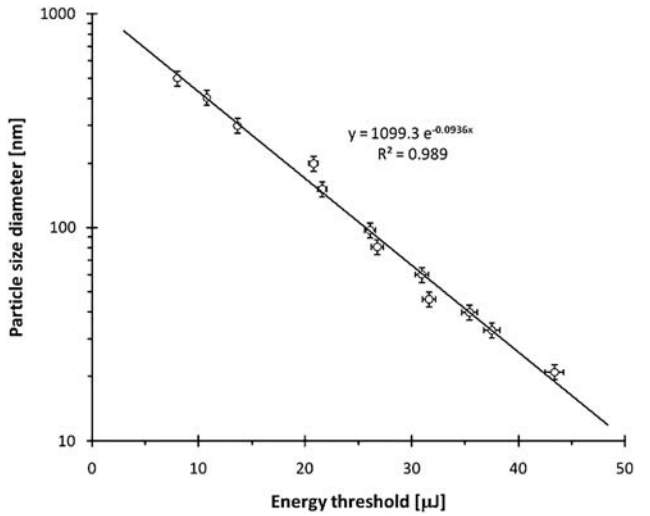

Fig. 6 Breakdown thresholds (BDP = 0.02) plotted as a function of particle diameter for a given set of polystyrene nanospheres with a diameter range from 21–499 nm.

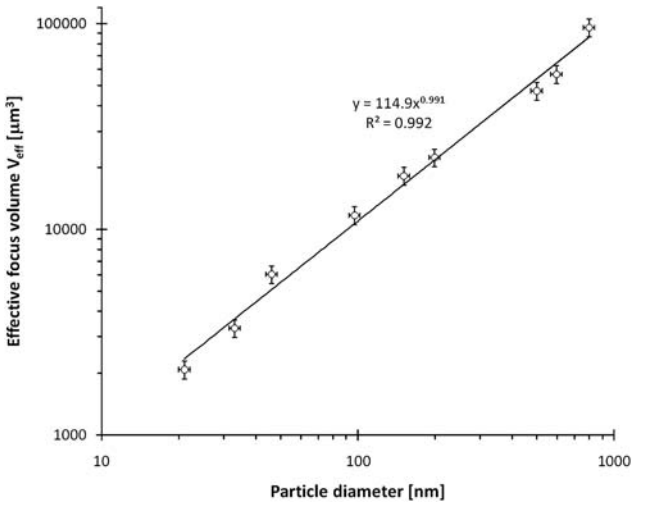

Fig. 7 Effective focus volume (V_{eff}) as a function of the particle diameter, determined for the concentration ranging from 2×10^7 to 2×10^8.

(spherical aberrations) of the focusing optics as shown by Walther *et al.*[11] and Walther and Hauser.[14] Nevertheless, the simplified approach can be used to derive empirical correlations between particle size and V_{eff}. According to Scherbaum *et al.*,[20] V_{eff} is given by eqn (2) and can be derived using standard materials of known size and concentration:

$$V_{eff} = V_{particle} \frac{\log(1 - BDP)}{\log(1 - c_{particle} \times V_{particle})} \quad (2)$$

The volume of that rotational ellipsoid (=V_{eff}) increases with increasing particle diameter (=decreasing power density required to ignite a plasma), increases with increasing laser energy, and most importantly, is independent of the particle number density for a wide range of concentrations.[21] Blank measurements using ultrapure water were used to derive the maximum energy, where still no plasma event occurred. This maximum energy was 86 ± 5 µJ recorded on the pyroelectric detector in front of the sample cell. Blank measurements showed an overall day-to-day variation of around 12%, and thus, the laser pulse energy was adjusted to 70 µJ. By applying this laser energy, using standard materials of know size and concentrations and measuring the respective BDP, V_{eff} can be calculated from eqn (3). As V_{eff} is independent of the particle concentrations (verified for particle concentrations relevant for this study) a direct relationship between V_{eff} and the particle concentration can be established (eqn (3), Fig. 7).

$$V_{eff} = 114.9 \times d_{particle}^{0.991} \quad (3)$$

with V_{eff} = effective focus volume, determined for 70 µJ, $d_{particle}$ = particle diameter (nm).

Comparing our results for V_{eff} with values given by Bundschuh *et al.*,[21] we find that the our values for V_{eff} are roughly a factor of 4 lower but with a comparable slope over the total fit curve. These can be again explained by the different instrumental setups, different water qualities, and the different lasers systems. Based on this calibration for the effective focus volume, the particle number density for unknown samples can be calculated after determination of the corresponding particle size (eqn (1)) and the respective BDP according to eqn (4):[21]

$$c_{particle} = \frac{1}{V_{particle}} \times \left(1 - (1 - BDP)^{V_{particle}/V_{eff}}\right) \quad (4)$$

4. Applications

4.1. Adsorption to storage vessels

To investigate whether the particle number and size are affected by the sample storage, long term experiments were conducted, using different sample container volumes and materials. We used laboratory glassware bottles (5 L, 1 L volume, SCHOTT AG, Mainz, Germany) as well as polyethylene bottles with different volumes (15 mL, 60 mL, 125 mL volume, NALGENE Labware, Rochester, USA) and collected raw lake water at the water works at Lengg (Lake Zurich, Switzerland). The LIBD system was transported to the water works for immediate analysis of water samples. Additional samples were transported back to the laboratory in a cool box and also during the whole study the samples were stored in the cool box (8 °C). After 7 and 90 days subsamples of all storage vessels were measured in the laboratory.

The energy curves of the subsamples from the 5 L and the 15 mL sample containers are given in Fig. 8 and the results are summarized in Table 1.

Generally, the size measurements are in good agreement with previous LIBD measurements for water samples from Lake Zurich, collected from the same sampling location.[22] The slopes of the energy curves became flatter with time, the effect being more pronounced in the case of the 15 mL sample compared to the 5 L sample. A decreasing slope indicates a decreasing particle number density which is also underlined by the results from Table 1. The initial concentration for the 5 L sample was 1.8×10^8 particles mL^{-1}, which is reduced to 1.2×10^8 particles mL^{-1} after 90 days corresponding to a relative loss of 35%. In the 15 mL sample, the concentration decreased from 1.9×10^8

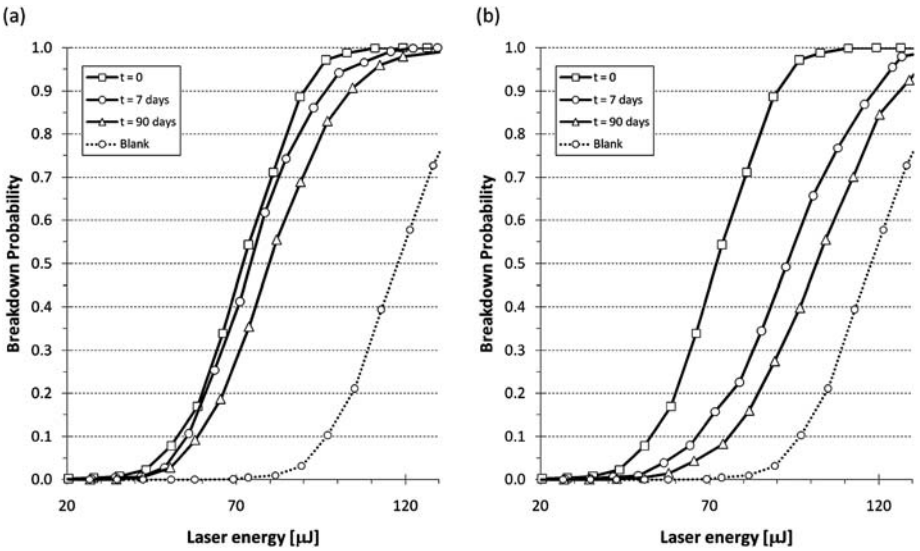

Fig. 8 Long-term experiments for different storage bottles containing lake water stored for 3 months [(a) 5 L and (b) 15 mL].

Table 1 Comparison of particle size and concentration for two storage bottles with different volumes (5 L and 15 mL)

	Particle size diameter/nm	Concentration/ particles mL^{-1}	Relative change of concentration (%)
5 L (glass)			
0 days	30 ± 4	1.79×10^8	100
7 days	26 ± 3	1.68×10^8	94
90 days	25 ± 5	1.16×10^8	65
15 mL (PE)			
0 days	29 ± 4	1.86×10^8	100
7 days	26 ± 5	6.47×10^7	35
90 days	22 ± 3	4.74×10^7	26

particles mL^{-1} down to 4.5×10^7 particles mL^{-1}, which corresponds to a relative loss of 74%. All energy curves rise at a similar level indicating that the particle size remains rather stable. Only in the longest run using the 15 mL storage vessel, the energy curve rises at a higher energy corresponding to smaller particle diameters. The same trend can also be observed for the samples from the 5 L container although the change in the particle size was within the measurement uncertainty. A shift to higher energies indicates a decreasing particle size which cannot be explained with diffusion losses to the samples container, or with the formation of aggregates, which would cause a decrease of the threshold energy E_{th}. However, the presence of larger particles in the raw water at the beginning of the experiment and the preferential settling of such particles during the experiment likely explain the increase of the E_{th} with time. Experiments performed with 60 mL and 125 mL containers showed similar trends of decreased NP concentrations and constant particle sizes over time.

The much higher loss in the case of the smaller storage vessel (15 mL) together with only minor changes in the particles size clearly indicates a sample loss *via* adsorption of particles to the walls of the storage vessels, underlining the advantage of rapid on-line analysis without sample storage.

4.2. On-line measurements at a drinking water plant

To test the applicability of the mobile LIBD system, we performed on-site measurements at the drinking water plant at Maennedorf, Lake Zurich, Switzerland using a flow-through sample cell, directly connected to the water reservoirs. The purification steps of the raw lake water include ozonation, activated carbon and ultrafiltration using multibore membranes (Multibore Membrane dizzer 5000, inge water technologies AG, Germany). The different treatment steps are briefly described in the following section.

The raw lake water is treated with ozone using an ozonation reactor (0.54 mg O_3 L^{-1}, Depolox) for disinfection and oxidation water constituents. Following ozonation, the water flow is directed to activated carbon reactors for adsorption of the remaining organic matter and micropollutants as well as for biodegradation of assimilable organic compounds produced during ozonation. Finally, the water is filtered using multibore membrane modules with a cutoff limit of 10 nm (100 kDa), which is sufficient to remove bacteria and viruses. These membranes are back-flushed as recovery-maintenance every 96 hours.

We analyzed the particle sizes and concentrations at four different sampling locations within the water works on-line (Lake water, ozonation, activated carbon, ultrafiltration). Each measurement was repeated three times. With the given instrumental setup, recording a complete energy curve with 30 individual data points and 2000 laser shots per data point took around 12 minutes. In addition to the water samples, ultrapure water was measured to determine instrumental background and blank levels.

The results for one set of experiments are given in Fig. 9 and summarized in Table 2. The ozonation resulted in a decrease of the particle number density by a factor of ~3 but did not significantly affect the particle diameters of the colloids in the water stream, indicated by the decreased slope and the constant onset of the energy curves. Bundschuh *et al.*[21] investigated different purification steps of a water works at lake Constance (Bodensee Zweckverbund, Germany). Also in their study, the

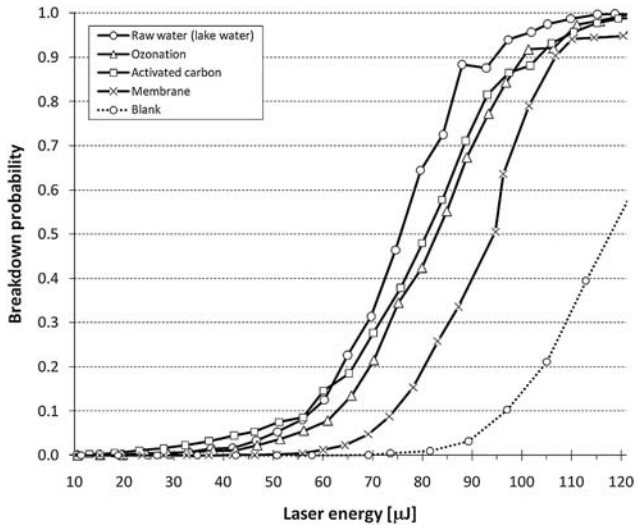

Fig. 9 On-line measurements at the drinking water plant (Maennedorf, Lake Zurich) after different water treatment steps.

Table 2 Particle size and particle number densities after different purification steps at the drinking water plant

Sample	Particle size, diameter/nm	Concentration/ particles mL^{-1}
Raw water	29 ± 4	$(12.2 \pm 0.98) \times 10^7$
Ozonation	22 ± 5	$(3.99 \pm 0.27) \times 10^7$
Activated carbon	73 ± 6	$(9.76 \pm 0.88) \times 10^7$
Ultrafiltration	11 ± 4	$(4.74 \pm 0.23) \times 10^7$

particle size remained constant and the particle number density was reduced by a factor of ~2.4 after ozonation was completed. The following treatment step by activated carbon increased the particle size from 22 ± 5 nm to 73 ± 6 nm clearly shown by the earlier rise of the energy curves. In addition, the particle number density increased from 4×10^7 particles mL^{-1} to 10×10^7 particles mL^{-1}. This clearly indicates that particles were washed out of the activated carbon. Whether these particles are small flocs consisting of biological materials grown within the activated carbon tank or whether they were inorganic carbon particles loosely attached to and washed off from the activated carbon is not clear. Ultrafiltration is used as the last purification step. The cutoff of the membrane is 100 kDa corresponding to roughly 10 nm. The particles in the permeate (after the membrane) had a diameter of 11 ± 4 nm, which is in excellent agreement with the reported cut-off diameter. In addition to a large decrease in size, reflected by the onset of the energy curves at higher energies, also the particle number density was reduced by about a factor of 2 down to 5×10^7 particles mL^{-1}. These results show that even after ultrafiltration, particle number concentrations in the drinking water are still rather high.

5. Conclusions

We presented an alternative method for the detection of a laser induced breakdown events by measuring the laser energy of individual pulses before and after passing through the measurement cell. Our system achieves similar figures of merit compared to the acoustic and optical detections. The simplified instrumental setup is well suited for field-based measurements and compared to the optical detection method also considerably less expensive.

After 3 months 75% and 35% of the NPs contained in raw lake water were adsorbed to the walls of 15 mL and 5 L sample containers, whereby the size of the particles remained rather constant. On-site measurements at a drinking water plant revealed an increase of the particle size from 20 nm to 75 nm after activated carbon treatment possibly caused by a release of organic fragments from the biology developed within the activated carbon reactor. The final ultrafiltration reduced the particle size to a diameter of 11 nm in good agreement with the 100 kD cutoff of the membrane. These results demonstrate the strength of the LIBD methods to detect relative changes in size and concentration of NP in aqueous systems.

Our system is operated at a higher repetition rate than other LIBD systems (100 Hz *vs.* 20 Hz) which enables recording transient signals with a time resolution in the order of a few seconds, by only measuring the BDP at a fixed energy. Although such data would not allow quantifying the size and the concentration of NP, relative changes in NP populations would be detected.

Acknowledgements

The authors wish to thank the Eawag Action Field Project Program and the Swiss National Science Foundation for the financial support and the ETH Zurich machine shop for their valuable technical help and construction of the mobile LIBD instrumental setup. Tobias Wagner and Birgit Hetzer (FZ Karlsruhe) are gratefully acknowledged for their valuable input which set the basis for the given LIBD system. Furthermore, the authors would like to thank Brian Sinnet and Jacqueline Traber (both Eawag) for their valuable assistance during the field-based measurements in this study.

Notes and references

1 L. Morawska, H. Wang, Z. Ristovski, E. R. Jayaratne, G. Johnson, H. C. Cheung, X. Ling and C. He, *J. Environ. Monit.*, 2009, **11**, 1758–1773.
2 T. M. Peters, S. Elzey, R. Johnson, H. Park, V. H. Grassian, T. Maher and P. O'Shaughnessy, *J. Occup. Environ. Hyg.*, 2009, **6**, 73–81.
3 M. Filella, J. W. Zhang, M. E. Newman and J. Buffle, *Colloids Surf., A*, 1997, **120**, 27–46.
4 M. Hassellov and R. Kaegi, in *Nanoscience and Nanotechnology: Environmental and Human Health Implications*, ed. J. R. Lead and E. Smith, Wiley, West Sussex, UK, 2008, pp. 211–266.
5 K. J. Wilkinson and J. R. Lead, *Environmental Colloids and Particles. Behavior, Separation and Characterization*, John Wiley & Sons Ltd, West Sussex, England, 2007.
6 T. Kitamori, K. Yokose, M. Sakagami and T. Sawada, *Jpn. J. Appl. Phys., Part 1*, 1989, **28**, 1195–1198.
7 T. Kitamori, K. Yokose, K. Suzuki, T. Sawada and Y. Gohshi, *Jpn. J. Appl. Phys., Part 2*, 1988, **27**, L983–L985.
8 W. Hauser, H. Geckeis, J. I. Kim and T. Fierz, *Colloids Surf., A*, 2002, **203**, 37–45.
9 T. Bundschuh, R. Knopp and J. I. Kim, *Colloids Surf., A*, 2001, **177**, 47–55.
10 T. Bundschuh, R. Knopp, R. Muller, J. I. Kim, V. Neck and T. Fanghanel, *Radiochim. Acta*, 2000, **88**, 625–629.

11 C. Walther, S. Buchner, M. Filella and V. Chanudet, *J. Colloid Interface Sci.*, 2006, **301**, 532–537.
12 C. Walther, H. R. Cho and T. Fanghanel, *Appl. Phys. Lett.*, 2004, **85**, 6329–6331.
13 J. I. Kim and C. Walther, in *Environmental Colloids and Particles. Behavior, Separation and Characterization*, ed. K. J. Wilkinson and J. R. Lead, John Wiley & Sons Ltd, West Sussex, England, 2007, vol. 10, p. 687.
14 C. Walther and W. Hauser, *Appl. Phys. B: Lasers Opt.*, 2009, **97**, 877–886.
15 C. Walther, C. Bitea, W. Hauser, J. I. Kim and F. J. Scherbaum, *Nucl. Instrum. Methods Phys. Res., Sect. B*, 2002, **195**, 374–388.
16 T. Bundschuh, W. Hauser, J. I. Kim, R. Knopp and F. J. Scherbaum, *Colloids Surf., A*, 2001, **180**, 285–293.
17 T. Bundschuh, T. Wagner, I. Eberhagen, B. Hambsch and R. Koster, *Spectrosc. – Int. J.*, 2005, **19**, 69–78.
18 T. U. Wagner, T. Bundschuh and R. Koster, *Part. Part. Syst. Charact.*, 2005, **22**, 181–191.
19 *German Pat.*, DE-19602048, 1999.
20 F. J. Scherbaum, R. Knopp and J. I. Kim, *Appl. Phys. B: Lasers Opt.*, 1996, **63**, 299–306.
21 T. Bundschuh, R. Knopp, R. Winzenbacher, J. I. Kim and R. Koester, *Acta Hydrochim. Hydrobiol.*, 2001, **29**, 7–15.
22 R. Kaegi, T. Wagner, B. Hetzer, B. Sinnet, G. Tzuetkov and M. Boller, *Water Res.*, 2008, **42**, 2778–2786.